New method to calculate the nuclear radius from low energy fusion and total reaction cross sections

K. C. C. Pires,* S. Appannababu, R. Lichtenthäler, and O. C. B. Santos
Departamento de Física Nuclear, Universidade de São Paulo, 05508-090, São Paulo, Brasil

(Received 28 March 2018; revised manuscript received 24 May 2018; published 23 July 2018)

We introduce a new method to calculate the nuclear radius from low energy fusion and total reaction cross section measurements. We apply it for several light stable and unstable projectiles on light mass targets (^{9}Be, ^{12}C, and ^{27}Al). Our results are in reasonable agreement with the radii obtained from high energy experimental data. We also interpreted the results as a function of the isospin of the projectile, mass of the interacting target, and neutron and proton numbers.

DOI: 10.1103/PhysRevC.98.014614

I. INTRODUCTION

With the advent of new accelerator facilities, there has been a great improvement in the study of reactions induced by radioactive ion beams, in order to investigate the effects of nuclear structure on reaction mechanisms [1–9]. Light nuclei located near or far from the line of stability usually exhibits exotic structures, such as a halo- or skin-like structure and the study of nuclear reactions with the exotic nuclei is very interesting due to their extended size and weakly bound cluster like structures. The weakly bound nature of these exotic nuclei results in a larger nuclear radii, which may result in the increased probabilities for specific reaction channels such as transfer or breakup [10–14]. It is well established that the nuclear interaction cross sections of the stable and unstable nuclei can be measured by using high energy heavy ion reactions [10]. The interacting radius can be deduced directly from the total reaction cross section (TRCS) measurements by using a geometric relation valid at high energies:

$$\sigma_R = \pi R_I^2, \tag{1}$$

where R_I is the interacting radius, which is the sum of the projectile and target radii ($R_I = R_p + R_t$) [15]. Moreover, the total reaction cross sections can be obtained directly from experiments or can be extracted by analyzing elastic scattering angular distributions using different model calculations [13,16]. More recently, several reports show that low energy elastic scattering measurements of systems involving exotic projectiles such as ^{6}He [11–14], ^{11}Li [17], ^{11}Be [18], and others, provide estimations of the TRCS. Elastic scattering measurements provide information about the strong nuclear potential as well as the total reaction cross sections [16]. However, TRCS are usually affected by couplings between elastic and other reaction channels such as fusion, transfer reactions, inelastic scattering, breakup, and so on. In general, in the elastic scattering of light nuclei at low energy, the fusion reaction is the one that contributes most significantly to the total reaction cross section. In case of very weakly bound exotic projectiles such as ^{6}He, ^{11}Li, ^{11}Be, and others, the breakup channel may have a relevant effect on the total reaction cross section. Scattering of these exotic nuclei on heavy targets are usually influenced by breakup reactions occurring in the long-range Coulomb field, far away from the short-range nuclear interaction. This long-range Coulomb breakup is induced by the strong dipole and quadrupole projectile polarizabilities and may contribute significantly to the total reaction cross sections, affecting the nuclear radius obtained directly from Eq. (1).

For light targets, on the other hand, the scattering at energies above the Coulomb barrier is dominated by the short-range nuclear interaction and the effect of the Coulomb breakup seems to be less important. Thus it seems to be possible to obtain information of the nuclear radius directly from total reaction cross section measurements using light targets.

In this paper, we propose a new method to obtain the projectile nuclear radius from fusion cross section measurements at low energy. We used total reaction cross section data where fusion data are not available.

The structure of this paper is organized as follows. Section II describes the method to obtain the nuclear radius using fusion and TRCS data. Section III presents the application of the method for several stable and unstable projectiles (^{6}He, ^{6,7,8}Li, ^{7,9}Be, ^{8,10}B, and ^{12}C) on ^{9}Be, ^{12}C, and ^{27}Al targets. Section IV interprets the results as a function of the isospin, proton and neutron numbers. Finally, Sec. V summarizes the conclusions.

II. METHODOLOGY

The energy dependence of the total reaction cross section at near barrier energies can be described by the well-known geometric formula [19]:

$$\sigma_R = \pi R_I^2 \left(1 - \frac{V_B}{E}\right), \tag{2}$$

where V_B is the Coulomb barrier height and it is only valid for $E > V_B$. Equation (2) is deduced from the exact formula: $\sigma_R = \frac{\pi}{k^2}\sum_0^{l_{\rm graz}}(2l+1)T(l)$, assuming a sharp cutoff transmission coefficient $T(l) = 1$ for $l \leqslant l_{\rm graz}$ and $T(l) = 0$ for $l > l_{\rm graz}$ a semiclassical relation for the grazing angular momentum:

*kelly@.if.usp.br

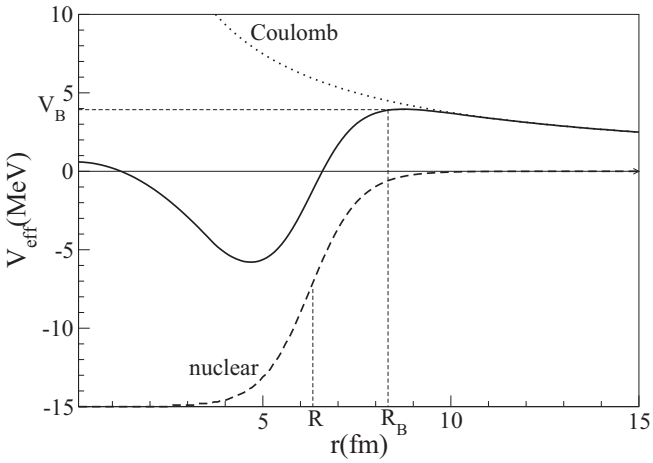

FIG. 1. Nuclear (dashed line), Coulomb (dotted line), and total effective (solid line) potentials as a function of the radius for a Woods-Saxon shape with $V_0 = 15$ MeV, $r_0 = 1.3$ fm, and $a = 0.65$ fm for the ^{6}He + ^{27}Al system. The position (R_B), height (V_B) of the Coulomb barrier and the nuclear radius (R) taken at one-half of the nuclear saturation value are shown.

$l_{\text{graz}} = R_I\sqrt{2\mu(E - V_B)}/\hbar$, where μ is the reduced mass of the system.

In the high energy limit, Eq. (2) can be simplified to Eq. (1). At low energies it takes into account the reduction of the reaction cross section due to the proximity of the Coulomb barrier.

Recently, it was found that the fusion cross sections of heavy systems are well reproduced by Eq. (2), provided that V_B and R_B ($R_I = R_B$, where R_B is the Coulomb barrier radius) are obtained from calculations for the short range nuclear potential using a double folding potential [20].

If the nuclear potential is known, the Coulomb barrier height V_B and position R_B can be obtained from Eq. (3) below:

$$\frac{d}{dr}[V_{\text{coul}}(r) + V_{\text{nucl}}(r)]_{r=R_B} = 0, \tag{3}$$

where $V_{\text{coul}}(r) = Z_1 Z_2 e^2/r$ and $V_{\text{nucl}}(r)$ is the real part of the short range nuclear interaction.

In Fig. 1, we plot $V_{\text{eff}} = V_{\text{nucl}}(r) + V_{\text{coul}}(r)$ for a Woods-Saxon nuclear potential and $l = 0$. In this figure we can see that the Coulomb barrier height V_B and radius R_B are fully determined by the nuclear potential in the surface region ($r > R$) and are not affected by its shape in the inner region ($r < R$).

Therefore, the tail of the short-range nuclear potential determines the Coulomb barrier parameters. In this way, the problem is simplified, since the nuclear potential takes the exponential form in the surface region. Considering a Woods-Saxon shape the tail of the potential reduces to $V \to V_0 e^{\frac{R}{a}} e^{\frac{-r}{a}}$ for $r \gg R$. In addition to this, in Ref. [20] it is shown that it is possible to reproduce the exponential tail of a double folding potential using a Woods-Saxon potential with the fixed geometry as $R = 1.3(A_1^{1/3} + A_2^{1/3})$, $a = 0.65$ fm and $V_0 \approx 15$ MeV. The use of a Woods-Saxon shape allows to obtain an analytical solution to Eq. (3) in the relevant region (see calculation details in Ref. [20]). Thus, the final expressions for V_B and R_B proposed by Ref. [20] are given by

$$V_B = \frac{Z_p Z_t e^2}{R_B} - \frac{15}{x+1}, \tag{4}$$

where x is a dimensionless parameter written as

$$x = \frac{27.1\left(A_p^{1/3} + A_t^{1/3}\right)^2}{Z_p Z_t}. \tag{5}$$

The relation between the nuclear radius R and the Coulomb barrier radius R_B is given by

$$R_B = R + 0.65\ln(x), \tag{6}$$

Formulas (4), (5), and (6) provide values for V_B and R_B compatible with the results obtained from numerical resolution of Eq. (3) using double folding potentials [20]. We see from the above equations that V_B and R_B basically depend on a single dimensionless parameter x, which is a simple function of the mass and charge of the colliding nuclei. In Ref. [20], the estimates from these formulas show a good agreement with the fusion cross section for stable systems at energies above the Coulomb barrier.

In addition, the above formulas allow an estimation of the nuclear radius in a inverse way, i.e., first the Coulomb barrier radius R_B is directly obtained from fusion cross section measurements using Eq. (2), and then the nuclear radius R is calculated from Eq. (6). As the dependence on V_B of Eq. (2) is only a correction, one can use V_B as obtained in zero order from Eq. (4) with R_B from Eq. (6) with $R = 1.3(A_1^{1/3} + A_2^{1/3})$. This allows us to adjust a single parameter R_B in Eq. (2) to fit fusion or total reaction cross section data.

It is to be noted that the nuclear radius R, as defined here, stands for the radius where the density of the nuclear matter falls to one-half of its saturation value.

III. RESULTS

A. Identical systems

As a first step, the new method to obtain the nuclear radius using fusion and total reaction cross sections was applied on ^{9}Be + ^{9}Be, ^{10}B + ^{10}B, and ^{12}C + ^{12}C identical systems [21–25]. For these systems there are available fusion and TRCS data as a function of the energy. The analysis was performed as follows: first the Coulomb barriers V_B were obtained in zero order using Eqs. (4), (5), and (6) with $R = 1.3(2A^{1/3})$ with $A_p = A_t = A$. Then, R_B was adjusted to best fit the TRCS (or fusion) data using Eq. (2). The error bar in R_B was estimated by varying the R_B value in order to produce two dashed curves, as shown in the figures. Finally, the nuclear radius R for the identical systems was calculated from Eq. (6), since $R = 2R(p)$ and then the projectile radius is obtained using $R(p) = R/2$.

Figure 2 shows the R_B best fits (solid lines) obtained using Eq. (2) with $R_B = 7.27$ fm and $R_B = 7.43$ fm, for ^{9}Be + ^{9}Be and ^{12}C + ^{12}C systems, respectively. The nuclear radius was calculated using Eq. (6) and the results are $R(p) = 2.53(23)$ fm for ^{9}Be and $R(p) = 2.82(28)$ fm for ^{12}C nucleus. This values are in good agreement with ones obtained by Tanihata *et al.* at high energy, reported as 2.45(1) fm and 2.61(2) fm for ^{9}Be

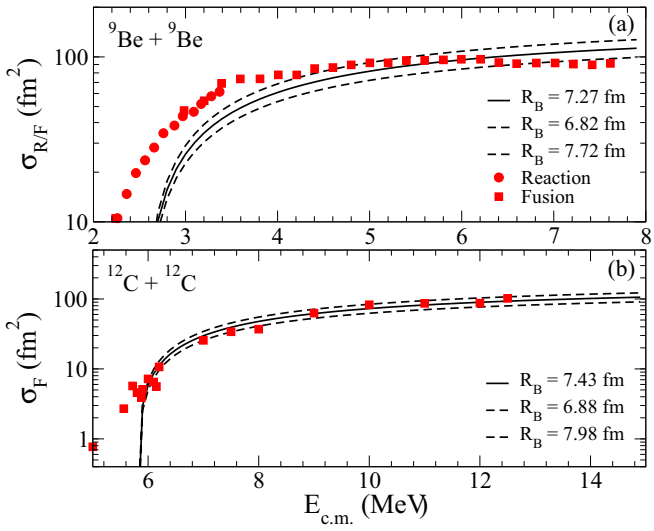

FIG. 2. Total fusion (solid squares) and total reaction (solid circles) cross section for (a) ^{9}Be + ^{9}Be and (b) ^{12}C + ^{12}C systems [21,22,24]. Solid lines are the R_B fits using Eq. (2) and the dashed lines provide an estimation of the R_B error bars.

and ^{12}C, respectively [10]. Furthermore, Ref. [26] presents the experimental root-mean-square (rms) nuclear charge radii for 909 isotopes of 92 elements from ^{1}H to ^{96}Cm, obtained by analysis of radii changes determined from optical and, to a lesser extent, K_α x-ray isotope shifts absolute radii measured by muonic spectra and electronic scattering experiments. In this case, the rms radius of the ^{9}Be and ^{12}C are reported as 2.52(1) fm and 2.47(2) fm [26], respectively.

Figure 3 shows the results for ^{10}B + ^{10}B (a) fusion [23] and (b) TRCS [25] data. The ^{10}B nuclear radius obtained from fusion cross section is $R = 1.95(15)$ fm and obtained from TRCS data is $R = 2.20(15)$ fm. Both values are however

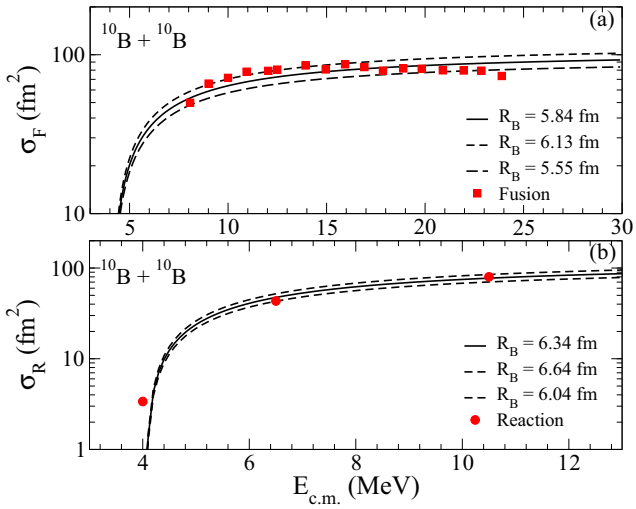

FIG. 3. (a) Total fusion and (b) total reaction cross sections for the ^{10}B + ^{10}B system [23]. The solid curves are the best R_B fits using Eq. (2) and the dashed lines provide an estimation of the R_B error bars.

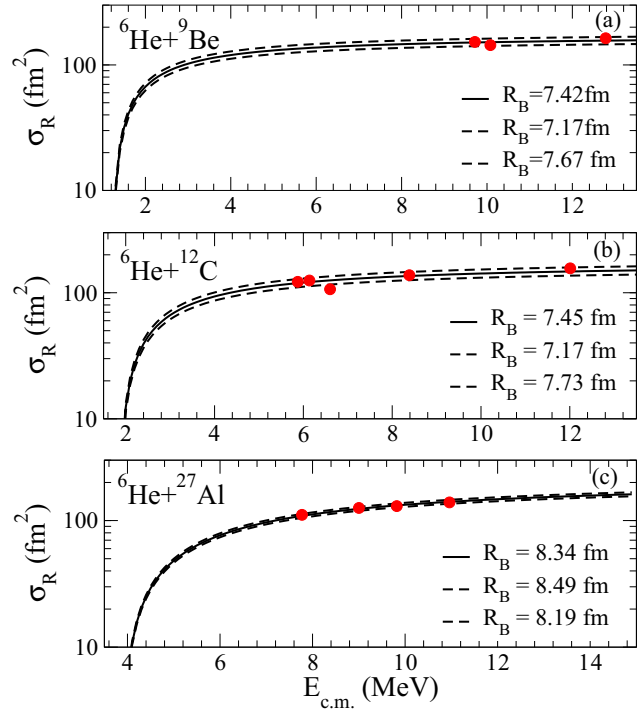

FIG. 4. Total reaction cross sections (solid circles) for (a) the ^{6}He + ^{9}Be system [13,43], (b) the ^{6}He + ^{12}C system [32], and (c) the ^{6}He + ^{27}Al system [39]. Solid line is the R_B fit using Eq. (2) and the dashed lines provide an estimation of the R_B error bars.

smaller than the rms radius value of $R = 2.43(5)$ fm reported in Ref. [26].

B. Application for He, Li, and Be projectiles

Once the radii of ^{9}Be and ^{12}C have been determined from data of identical systems, it is possible to apply this method to data of non-identical systems involving ^{9}Be and ^{12}C targets with different projectiles, in order to obtain the projectile radius. We apply it to ^{6}He, ^{6,7,8}Li, ^{7,9}Be, and ^{8,10}B on ^{9}Be, ^{12}C, and ^{27}Al targets. For ^{27}Al the radius was assumed to be $R = r_0 A^{1/3}$, where r_0 is taken as 1.3 fm and $A = 27$. No error was assumed for the ^{27}Al radius.

The total reaction cross sections were obtained directly from available elastic scattering angular distributions [13,21,24,25,27–40]. When several results of total reaction cross sections were available for the same system, the average value and standard deviations were used. As described in Sec. III A, the fusion or TRCS data were fitted to obtain R_B. Then, the nuclear radius R was calculated from Eq. (6). Since $R = R(p) + R(t)$, the projectile radius is obtained by $R(p) = R - R(t)$, where $R(t)$ is the target radius determined in Sec. III A.

Figures 4, 5, 6, 7, 8, 9, and 10 show the results of R_B fit for all systems studied. In particular, the total reaction cross section for the ^{6}Li + ^{9}Be system was extracted by using three different approaches: Woods-Saxon, São Paulo potential [41,42], and collective model [30] formalisms. The last one interprets the excitations in terms of the deformation of the charge and/or

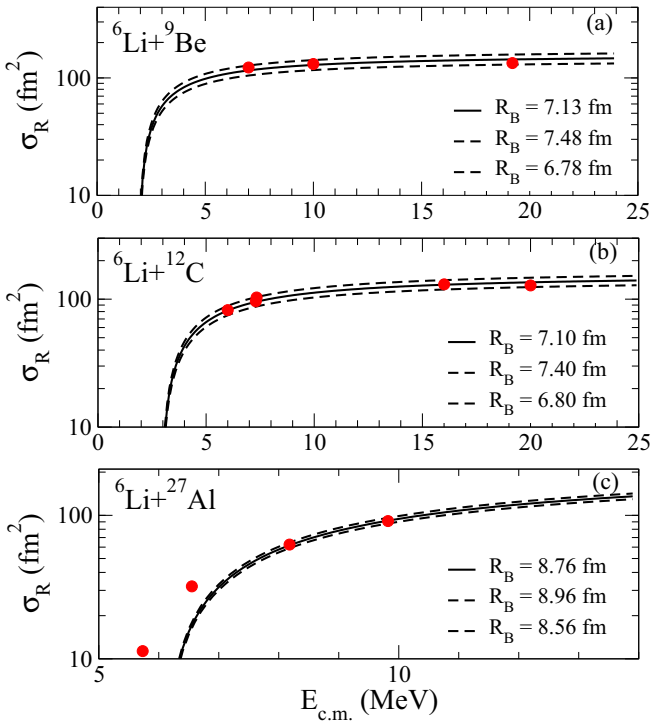

FIG. 5. Total reaction cross sections (solid circles) for (a) the ^{6}Li + ^{9}Be system [30,44–46], (b) the ^{6}Li + ^{12}C system [33,34], and (c) the ^{6}Li + ^{27}Al system [39]. Solid line is the R_B fit using Eq. (2) and the dashed lines provide an estimation of the R_B error bars.

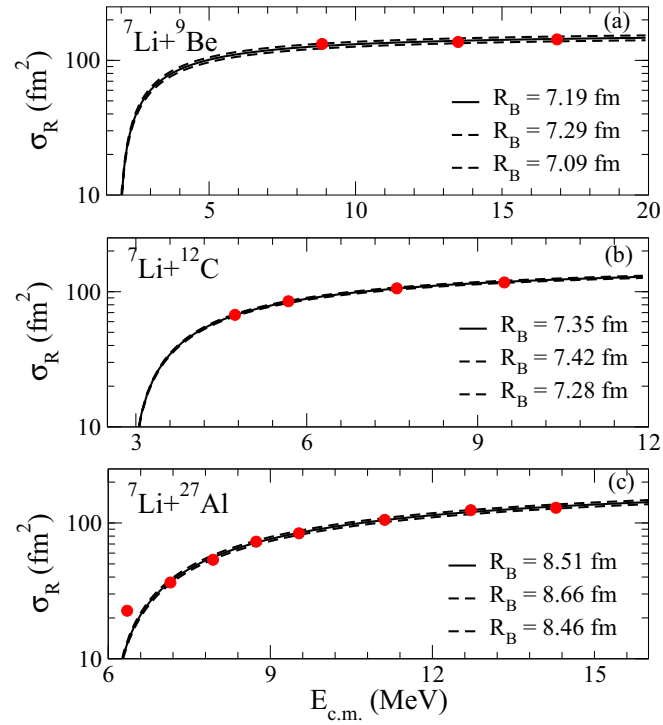

FIG. 7. Total reaction cross sections (solid circles) for (a) the ^{7}Li + ^{9}Be system [27], (b) the ^{7}Li + ^{12}C system [36], and (c) the ^{7}Li + ^{27}Al system [39]. Solid line is the R_B fit using Eq. (2) and the dashed lines provide an estimation of the R_B error bars.

mass distribution of the nuclei [30]. Compatible results of total reaction cross sections were obtained for the same energy and the average values with respective standard deviations were used. The results are shown in Fig. 5.

Table I presents the results for R_B, R, the projectile radius $R(p)$ for all analysed systems. The reduced radii [$r_0 = R(p)/A_p^{1/3}$] were also calculated and the results are shown in Table I.

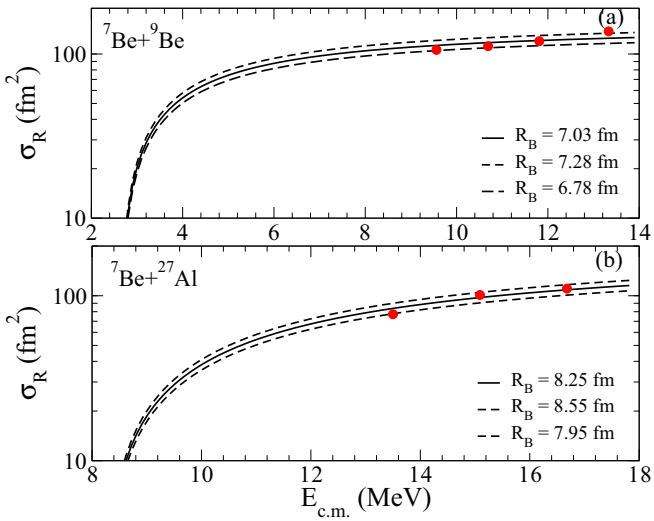

FIG. 6. Total reaction cross sections (solid circles) for (a) the ^{7}Be + ^{9}Be system [27,47] and (b) the ^{7}Be + ^{27}Al system [48]. Solid line is the R_B fit using Eq. (2) and the dashed lines provide an estimation of the R_B error bars.

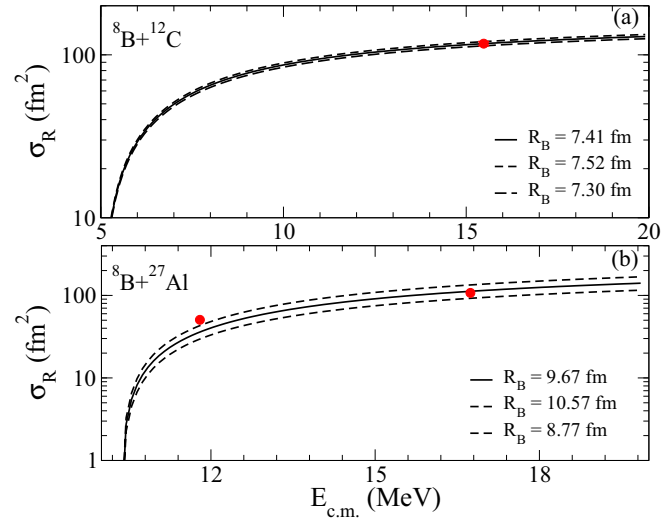

FIG. 8. Total reaction cross sections (solid circles) for (a) the ^{8}B + ^{12}C system [37] and (b) the ^{8}B + ^{27}Al system [28]. Solid line is the R_B fit using Eq. (2) and the dashed lines provide an estimation of the R_B error bars.

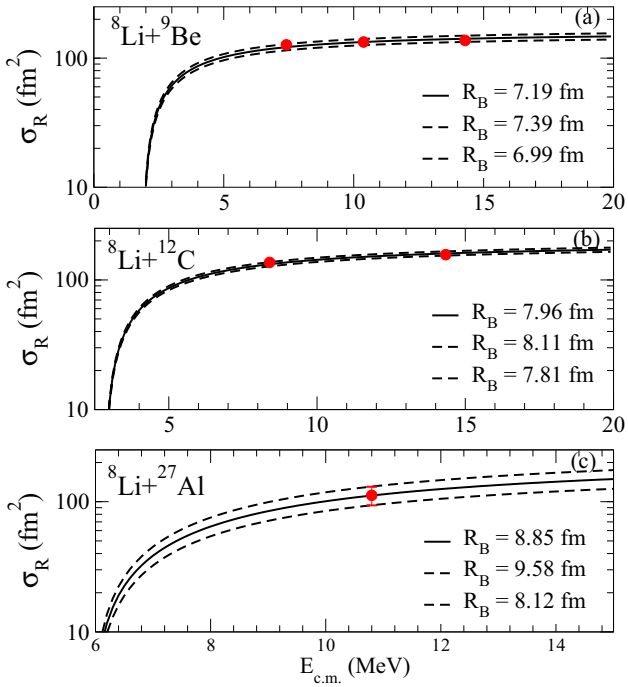

FIG. 9. Total reaction cross sections (solid circles) for (a) the ^{8}Li + ^{9}Be system [28,29,31], (b) the ^{8}Li + ^{12}C system [28,35], and (c) the ^{8}Li + ^{27}Al system [28]. Solid line is the R_B fit using Eq. (2) and the dashed lines provide an estimation of the R_B error bars.

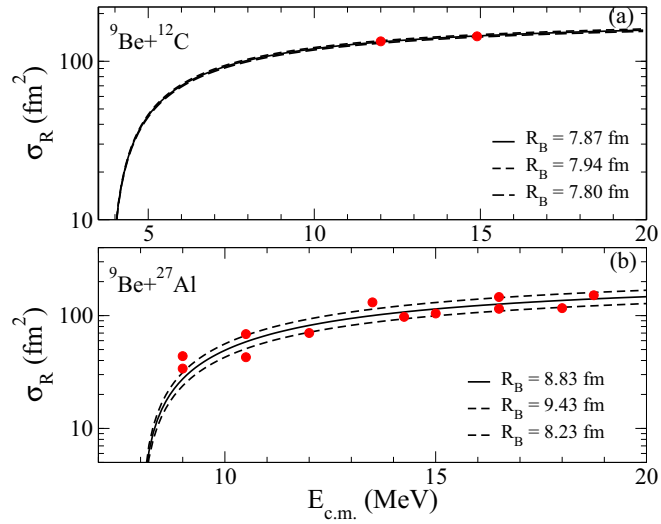

FIG. 10. Total reaction cross sections (solid circles) for (a) the ^{9}Be + ^{12}C system [38] and (b) the ^{9}Be + ^{27}Al system [49]. Solid line is the R_B fit using Eq. (2) and the dashed lines provide an estimation of the R_B error bars.

As far as the errors of the method are concerned a comment is necessary. The R_B error is propagated to R in formula (6) and then the projectile radius, as mentioned before, is determined from equation $R(p) = R - R(t)$. The error propagation

TABLE I. Coulomb barrier energy in the center of mass system (V_B), Coulomb barrier radius (R_B), x parameter [see Eq. (5)], nuclear radius (R), projectile radius [$R(p)$], projectile radius obtained from literature [$R(p)^{\text{lit}}$], projectile reduced radius [$r_0 = R(p)/A(p)^{1/3}$], and a list of references for the total reaction and fusion cross sections used in this calculations.

System	V_B (MeV)	R_B (fm)	x	R (fm)	$R(p)$ (fm)	$R(p)^{\text{lit}}$	r_0 (fm)	Refs.
^{9}Be + ^{9}Be	2.53	7.27(45)	29.31	5.07(45)	2.53(23)	2.45(1) [10]	1.22(11)	[21,22]
^{6}He + ^{9}Be	1.22	7.42(25)	51.45	4.85(25)	2.32(34)	2.48(1) [50–52]	1.28(19)	[13,43]
^{6}Li + ^{9}Be	1.92	7.13(35)	34.30	4.83(35)	2.30(42)	2.09(2) [10]	1.27(23)	[30,44–46]
^{7}Li + ^{9}Be	1.89	7.19(10)	36.01	4.86(10)	2.32(25)	2.23(2) [10]	1.21(13)	[27]
^{7}Be + ^{9}Be	2.61	7.03(25)	27.01	4.88(25)	2.35(34)	2.22(2) [10]	1.23(18)	[27,47]
^{8}Li + ^{9}Be	1.87	7.19(20)	37.59	4.83(20)	2.29(30)	2.36(2) [10]	1.15(15)	[28,29,31]
^{12}C + ^{12}C	5.80	7.43(55)	15.78	5.64(55)	2.82(28)	2.61(2) [10] 2.47(2) [26]	1.23(12)	[24]
^{6}He + ^{12}C	1.86	7.45(28)	38.08	5.08(28)	2.26(39)	2.18(2) [10] 2.21(6) [15]	1.25(22)	[32]
^{6}Li + ^{12}C	2.92	7.10(30)	25.39	4.99(30)	2.18(41)		1.20(23)	[33,34]
^{7}Li + ^{12}C	2.87	7.35(7)	26.59	5.22(7)	2.40(29)		1.25(15)	[36]
^{8}Li + ^{12}C	2.83	7.96(15)	27.70	5.80(15)	2.98(32)		1.49(16)	[28,35]
^{8}B + ^{12}C	4.98	7.41(11)	16.62	5.58(11)	2.76(30)		1.38(15)	[37]
^{9}Be + ^{12}C	3.84	7.87(07)	21.56	5.87(07)	3.05(29)	2.52(1) [26]	1.47(14)	[38]
^{6}He + ^{27}Al	3.90	8.34(15)	24.19	6.27(15)	2.37(15)	2.59 [53]	1.30(8)	[39]
^{6}Li + ^{27}Al	6.08	8.76(20)	16.12	6.95(20)	3.05(20)		1.68(11)	[39]
^{7}Li + ^{27}Al	5.99	8.51(15)	16.77	6.68(15)	2.78(15)		1.45(9)	[39]
^{8}Li + ^{27}Al	5.90	8.85(73)	17.37	6.99(73)	3.09(73)		1.55(37)	[28]
^{7}Be + ^{27}Al	8.22	8.25(30)	12.58	6.60(30)	2.70(30)		1.41(16)	[48]
^{9}Be + ^{27}Al	7.99	8.83(60)	13.45	7.14(60)	3.24(60)		1.56(29)	[49]
^{8}B + ^{27}Al	10.35	9.67(90)	10.42	8.15(90)	4.25(90)		2.12(45)	[28]
^{10}B + ^{10}B	4.06	5.84(29)	20.13	3.88(29)	1.95(15)	2.43(5) [26]	0.90(7)	[23]
^{10}B + ^{10}B	4.06	6.34(30)	20.13	4.39(30)	2.20(15)	2.43(5) [26]	1.02(7)	[25]

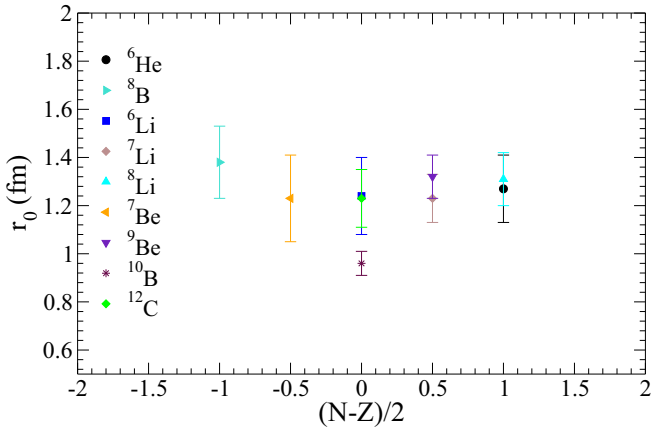

FIG. 11. Reduced radii of different stable and unstable nuclei as a function of isospin.

becomes critical here since, if the errors in $R(t)$ are large, they will propagate it to $R(p)$. In cases where $R(p) = R(t)$, as the ^{9}Be + ^{9}Be and ^{12}C + ^{12}C, we have $R(p) = R/2$ and the propagation does not affect much the relative errors. But, if $R(t) > R(p)$ this effect may become critical, introducing prohibitive errors to the projectile radius determination.

In particular, a weighted average with ^{9}Be and ^{12}C targets was used to obtain the radius for the ^{6}He projectile. The result is $R = 2.29(26)$ fm, in agreement with the previous reports of ^{6}He radius [10,15,52–54].

IV. NUCLEAR RADIUS AS A FUNCTION OF PROJECTILE ISOSPIN, TARGET MASS, PROJECTILE NEUTRON, AND PROTON NUMBERS

The present results were systematically analysed by plotting the reduced radius r_0 of the different stable and unstable nuclei on light targets (^{9}Be, ^{12}C, and ^{27}Al) as a function of (i) isospin of the projectile, (ii) mass of the target, (iii) projectile neutron number (for a fixed proton number), and (iv) projectile proton number (for a fixed neutron number). Here, the projectile isospin is defined as $(N - Z)/A$, where A is the mass, N is the neutron number, and Z is the proton number.

Figure 11 presents r_0 as a function of the isospin. One can also observe that near the line of stability (isospin smaller than 1/2) the nuclear radius tends to be smaller and increasing slightly for nonzero isospin. Despite the large error bars, this may be an indication that nuclei along the stability valley tend to have radii smaller than nuclei away from the stability valley.

We have tried to interpret the results by plotting the reduced radius for the same projectile as a function of the mass of the targets (^{9}Be, ^{12}C, and ^{27}Al). The results are shown in Fig. 12 and one can clearly observe that the radius of the projectile is not so independent of the interacting target mass. Furthermore, the same projectile on ^{9}Be and ^{12}C targets provides reasonably compatible results, showing the validity of our method. On the other hand, the r_0 obtained with ^{27}Al target shows, for some projectiles, values that are higher than the ones obtained from ^{9}Be and ^{12}C targets. This may be considered a limitation of our method when the mass number (A) becomes large.

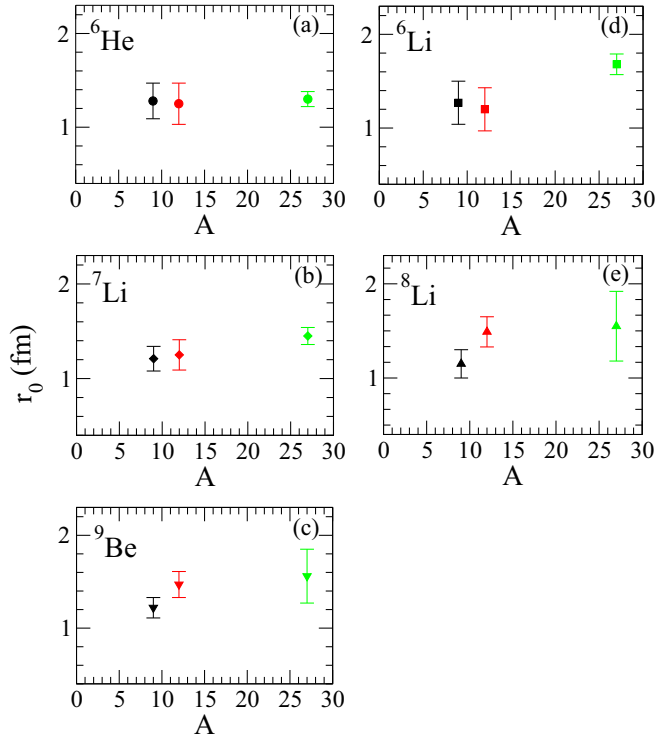

FIG. 12. Reduced radii of different projectiles plotted as a function of mass of the targets. Black points represents the ^{9}Be target, red points the ^{12}C target, and green points the ^{27}Al target.

As previously mentioned, for heavier targets, reactions in the Coulomb field may become more important, affecting the TRCS and consequently the radius estimations. In this cases, fusion cross sections should be used instead of TRCS.

Finally, Fig. 13 shows the reduced radius r_0 as a function of N (fixing Z) and Z (fixing N).

Even though the error bars are large, one can observe that, for the equal number of neutrons and protons, the nucleus

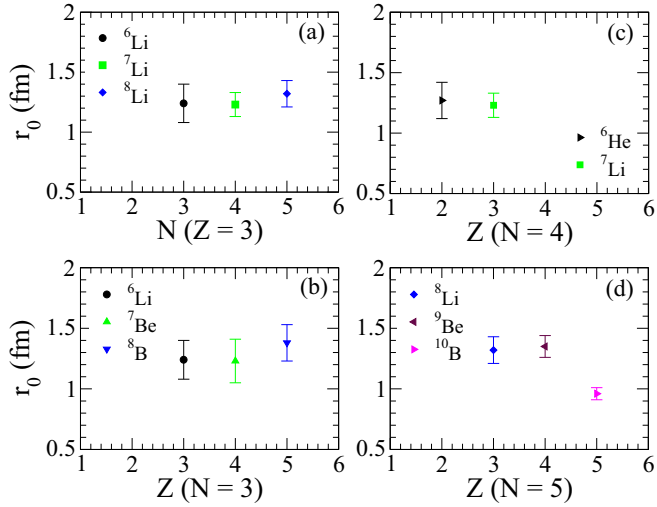

FIG. 13. Reduced radii of different nuclei as a function of Z (fixed N) and N (fixed Z).

seems to be more tightly packed, indicating that the nuclear radius is smaller in this configuration. From Fig. 13(a) for a fixed Z is possible to observe a small increase in the size of the nuclei according to the neutron number increase. Similarly, from Fig. 13(b) one can observe an identical result for a fixed N.

V. SUMMARY AND CONCLUSIONS

We presented a simple formalism to determine the nuclear radius from low energy fusion cross section data. When fusion data are not available, total reaction cross section data were used. We applied this methodology to several stable and unstable light nuclei interacting on light targets. The present results are in reasonable agreement with the radii obtained from reactions at high energies. Further, similar results were obtained for the same projectiles on different targets prove the reliability of this method.

It is observed that there is a slight tendency of the reduced radius, as a function of the isospin, showing an increase for nuclei away from the stability valley. The observed effects are small and similar to the error bars, however they may indicate a slight increasing trend of the nuclear radius for exotic projectiles such as ^{6}He and ^{8}B.

The present method is applicable to light systems at energies above the Coulomb barrier. At energies on the top of the Coulomb barrier and below, other effects due to coupled channels may become important, which are not accounted by the simple formula presented here. For heavier systems the effect of reactions in the long range Coulomb field certainly affects considerably the total reaction cross sections.

Indeed, for weakly bound and exotic projectiles there are indications that the complete fusion process may be suppressed above the Coulomb barrier. A possible explanation for this reduction is due to the breakup of the projectile prior to the fusion process. If the projectile breaks before it fuses with the target, it would enhance the barrier for the fragments and eventually reduce the complete fusion probability. Suppressions of about 30% have been observed for ^{6,7}Li and ^{9}Be projectiles on medium mass and heavy targets [55]. In this case, one should use the total fusion (complete + incomplete) instead of the complete fusion to extract the radius.

Given the simplicity of the method, we believe it is a useful tool to estimate the nuclear radius from cross section measurements at low energies. On the other hand, the method is a tool that provides good estimations of the fusion cross sections for stable systems at energies above the Coulomb barrier.

ACKNOWLEDGMENTS

The authors thank the Fundação de Amparo á Pesquisa do Estado de São Paulo (FAPESP), Procs. No. 2013/22100-7, No. 2014/19666-1, No. 2016/21434-7 and for CNPq for the financial support.

[1] N. Keeley, N. Alamanos, K. Kemper, and K. Rusek, Prog. Part. Nucl. Phys. **63**, 396 (2009).
[2] N. Keeley, R. Raabe, N. Alamanos, and J. Sida, Prog. Part. Nucl. Phys. **59**, 579 (2007).
[3] R. Lichtenthäler *et al.*, Eur. Phys. J. A **25**, 733 (2005).
[4] A. Lépine-Szily, R. Lichtenthäler, and V. Guimarães, Eur. Phys. J. A **50**, 128 (2014).
[5] B. B. Back, H. Esbensen, C. L. Jiang, and K. E. Rehm, Rev. Mod. Phys. **86**, 317 (2014).
[6] L. Canto, P. Gomes, R. Donangelo, J. Lubian, and M. Hussein, Phys. Rep. **596**, 1 (2015).
[7] P. R. S. Gomes *et al.*, Few-Body Syst. **57**, 165 (2016).
[8] J. J. Kolata, V. Guimarães, and E. F. Aguilera, Eur. Phys. J. A **52**, 123 (2016).
[9] R. Lichtenthäler, M. A. G. Alvarez, A. Lépine-Szily, S. Appannababu, K. C. C. Pires, U. U. da Silva, V. Scarduelli, R. P. Condori, and N. Deshmukh, Few-Body Syst. **57**, 157 (2016).
[10] I. Tanihata, H. Hamagaki, O. Hashimoto, Y. Shida, N. Yoshikawa, K. Sugimoto, O. Yamakawa, T. Kobayashi, and N. Takahashi, Phys. Rev. Lett. **55**, 2676 (1985).
[11] P. N. de Faria *et al.*, Phys. Rev. C **81**, 044605 (2010).
[12] V. Morcelle *et al.*, Phys. Lett. B **732**, 228 (2014).
[13] K. C. C. Pires *et al.*, Phys. Rev. C **83**, 064603 (2011).
[14] P. Mohr *et al.*, Phys. Rev. C **82**, 044606 (2010).
[15] I. Tanihata *et al.*, Phys. Lett. B **160**, 380 (1985).
[16] K. C. C. Pires, R. Lichtenthäler, A. Lépine-Szily, and V. Morcelle, Phys. Rev. C **90**, 027605 (2014).
[17] J. P. Fernández-García *et al.*, Phys. Rev. Lett. **110**, 142701 (2013).
[18] A. Di Pietro *et al.*, Phys. Rev. Lett. **105**, 022701 (2010).
[19] P. Frobrich and R. Lipperheide, *Theory of Nuclear Reactions* (Oxford University Press Inc., New York, 1996), p. 282.
[20] A. S. Freitas, L. Marques, X. X. Zhang, M. A. Luzio, P. Guillaumon, R. P. Condori, and R. Lichtenthäler, Braz. J. Phys. **46**, 120 (2016).
[21] A. Mukherjee and B. Dasmahapatra, Nucl. Phys. A **614**, 238 (1997).
[22] F. Lahlou, B. Cujec, and B. Dasmahapatra, Nucl. Phys. A **486**, 189 (1988).
[23] A. Szanto de Toledo, M. M. Coimbra, N. Added, R. M. Anjos, N. Carlin Filho, L. Fante, M. C. S. Figueira, V. Guimares, and E. M. Szanto, Phys. Rev. Lett. **62**, 1255 (1989).
[24] E. Almqvist, J. A. Kuehner, D. McPherson, and E. W. Vogt, Phys. Rev. **136**, B84 (1964).
[25] G. Dietl, G. Gruber, H. Schmidt-Böcking, and K. Bethge, Nucl. Phys. A **250**, 322 (1975).
[26] I. Angeli and K. Marinova, At. Data Nucl. Data Tables **99**, 69 (2013).
[27] S. Verma *et al.*, Eur. Phys. J. A **44**, 385 (2010).
[28] F. D. Becchetti *et al.*, Phys. Rev. C **48**, 308 (1993).
[29] V. Guimarães *et al.*, Phys. Rev. C **75**, 054602 (2007).
[30] E. Muskat, J. Carter, R. Fearick, and V. Hnizdo, Nucl. Phys. A **581**, 42 (1995).
[31] S. Mukherjee *et al.*, Eur. Phys. J. A **45**, 23 (2010).
[32] E. F. Aguilera, I. Martel, A. M. Sánchez-Benítez, and L. Acosta, Phys. Rev. C **83**, 021601(R) (2011).
[33] J. E. Poling, E. Norbeck, and R. R. Carlson, Phys. Rev. C **13**, 648 (1976).

[34] D. E. Trcka, A. D. Frawley, K. W. Kemper, D. Robson, J. D. Fox, and E. G. Myers, Phys. Rev. C **41**, 2134 (1990).
[35] A. Barioni *et al.*, Phys. Rev. C **80**, 034617 (2009).
[36] V. Parkar, K. Mahata, S. Santra, S. Kailas, A. Shrivastava, K. Ramachandran, A. Chatterjee, V. Jha, and P. Singh, Nucl. Phys. A **792**, 187 (2007).
[37] A. Barioni *et al.*, Phys. Rev. C **84**, 014603 (2011).
[38] J. C. Zamora *et al.*, Phys. Rev. C **84**, 034611 (2011).
[39] E. Benjamim *et al.*, Phys. Lett. B **647**, 30 (2007).
[40] P. R. S. Gomes *et al.*, Phys. Rev. C **70**, 054605 (2004).
[41] L. C. Chamon, B. V. Carlson, L. R. Gasques, D. Pereira, C. De Conti, M. A. G. Alvarez, M. S. Hussein, M. A. Cândido Ribeiro, E. S. Rossi, and C. P. Silva, Phys. Rev. C **66**, 014610 (2002).
[42] L. C. Chamon, D. Pereira, M. S. Hussein, M. A. Cândido Ribeiro, and D. Galetti, Phys. Rev. Lett. **79**, 5218 (1997).
[43] M. Majer *et al.*, Eur. Phys. J. A **43**, 153 (2010).
[44] J. Cook, Nucl. Phys. A **388**, 153 (1982).
[45] J. Cook and K. W. Kemper, Phys. Rev. C **31**, 1745 (1985).
[46] P. L. Von Behren, E. Norbeck, and G. L. Payne, Phys. Rev. C **10**, 550 (1974).
[47] K. C. C. Pires, Estudo de sistemas de núcleos exóticos leves 6He,7Be+9Be, Ph.D. thesis, Instituto de Física da Universidade de São Paulo, 2011.
[48] K. Kalita *et al.*, Phys. Rev. C **73**, 024609 (2006).
[49] G. V. Martí *et al.*, Phys. Rev. C **71**, 027602 (2005).
[50] J. S. Al-Khalili, J. A. Tostevin, and I. J. Thompson, Phys. Rev. C **54**, 1843 (1996).
[51] J. Tostevin, R. Johnson, and J. Al-Khalili, Nucl. Phys. A **630**, 340 (1998).
[52] B. V. Danilin, S. N. Ershov, and J. S. Vaagen, Phys. Rev. C **71**, 057301 (2005).
[53] S. Karataglidis, P. J. Dortmans, K. Amos, and C. Bennhold, Phys. Rev. C **61**, 024319 (2000).
[54] A. de Vismes *et al.*, Phys. Lett. B **505**, 15 (2001).
[55] M. Dasgupta, P. R. S. Gomes, D. J. Hinde, S. B. Moraes, R. M. Anjos, A. C. Berriman, R. D. Butt, N. Carlin, J. Lubian, C. R. Morton, J. O. Newton, and A. Szanto de Toledo, Phys. Rev. C **70**, 024606 (2004).